A Coupled Air–Sea–Monsoon Oscillator for the Tropospheric Biennial Oscillation

TIM LI

Department of Meteorology and International Pacific Research Center, University of Hawaii, Honolulu, Hawaii

C.-W. THAM AND C.-P. CHANG

Department of Meteorology, Naval Postgraduate School, Monterey, California

(Manuscript received 7 December 1999, in final form 10 May 2000)

ABSTRACT

The cause of the tropospheric biennial oscillation (TBO) in a simple coupled ocean–atmosphere model is examined. The model is first reduced to a pair of coupled linear first-order differential equations, piecewise in time, for analysis. It is found that two ingredients are essential for the biennial oscillation in the model. The first ingredient is the amplification of SST perturbations in both the Indian Ocean and western Pacific in opposite directions during the northern autumn, winter, and spring seasons, reflecting a positive feedback process. The second ingredient is the decay and change of signs of the SST anomaly in the western Pacific during the northern summer, representing a negative feedback process. Under such a scenario, the simple model exhibits a regular biennial oscillation.

Diagnosis of the model TBO reveals that the western Pacific SST and zonal wind anomalies have a lagged correlation at a timescale of 2–3 months, similar to observations. Such a phase lag results from both remote and local ocean–atmosphere–land interaction processes. The remote processes involve the large-scale east–west circulation associated with anomalous monsoon heating, whereas the local processes include the ocean horizontal and vertical advection and surface wind–evaporation–SST feedback. It is concluded that the phase lag between the SST and wind is a result rather than a cause of the TBO.

Oscillatory and nonoscillatory regimes of the model's solutions are obtained with the tuning of key parameters within realistic ranges. It is found that the model TBO is sensitive to both internal air–sea coupling coefficients and external basic-state parameters. With the slight change of these parameters, the model may undergo a bifurcation from a TBO regime to a chaotic regime or an annual oscillation regime—a possible scenario for the TBO irregularity. In particular, with a specification of interdecadal change of the basic-state wind, the model may undergo a continuous warming pattern in the eastern Pacific, resembling the prolonged El Niño condition in the early 1990s.

1. Introduction

Long-term observational data analyses reveal that the interannual rainfall variability over the Asian and Australian monsoon regions has a remarkable biennial spectrum peak (e.g., Lau and Shen 1988). These tropospheric biennial oscillation (TBO) signals have been detected in the rainfall of Indonesia (Yasunari and Suppiah 1988), India (Mooley and Parthasarathy 1984; Lau and Yang 1996), and East Asia (Tian and Yasunari 1992; Shen and Lau 1995; Chang et al. 2001). As a part of the coupled system, the rainfall TBO is associated with the variations in large-scale tropospheric circulation and tropical sea surface temperature (SST) patterns (Rasmusson and Carpenter 1982; Meehl 1987; Yasunari 1990; Ropelewski et al. 1992).

The observational discoveries have led to further theoretical understanding in terms of what causes the TBO. Air–sea interaction over the equatorial basins has been thought to be a key ingredient for the TBO. So far there have been various attempts to model the biennial oscillation by considering atmosphere–ocean feedbacks within the Tropics. First, Brier (1978) used state diagrams to demonstrate that a biennial oscillation can be achieved when a negative feedback between the atmosphere and the ocean is considered. Next, Nicholls (1978, 1979, 1984) simulated a TBO with a pair of first-order linear differential equations (one for the atmosphere and the other for ocean) in which the atmospheric pressure (wind) anomaly has an opposite impact on the SST anomaly (SSTA) during winter and summer, owing to the seasonal cycle of the basic-state wind. Based on schematic arguments (with addition of the long-lasted

Corresponding author address: Prof. Tim Li, Department of Meteorology/IPRC, University of Hawaii, 2525 Correa Rd., Honolulu, HI 96822.
E-mail: li@soest.hawaii.edu

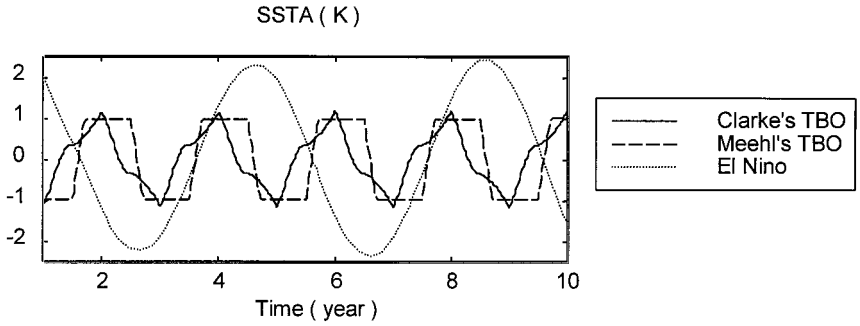

FIG. 1. Time series of SST anomalies associated with C98's TBO [Eqs. (1.1)–(1.2)], M87's TBO [Eqs. (1.1)–(1.3)], and El Niño delayed oscillation [Eqs. (1.1)–(1.4)].

ocean memory assumption), Meehl (1987, hereafter M87) gave a qualitative account of how a local negative air–sea feedback (feedback that involves local surface wind, evaporation, and ocean mixing processes) can lead, in the course of seasonal progression of maximum convection, to a biennial oscillation.

Recently, Clarke et al. (1998, hereafter C98) disputed the M87 seasonal maximum convection progression hypothesis by arguing that the peak phase of convection/wind associated with TBO is not in agreement with its seasonal maximum. Following the original idea of Nicholls (1978), they constructed a thermodynamic SST equation with the surface wind–evaporation feedback as a core process and a specification of seasonally varying basic-state winds. The key difference is that in the C98 model, the atmospheric differential equation is replaced with a time lag relationship between the anomalous wind and SST. The argument given is that the atmosphere responds rapidly to the ocean surface temperature and hence is better modeled with a time lag of 1–3 months than with a time-differential relation (which would imply a 6-month phase lag for a 2-yr oscillation period). The resulting equation is essentially a delayed differential equation of the form

$$\frac{\partial}{\partial t}T = k(t)T(t - \Delta), \tag{1.1}$$

where t is time, T the anomalous SST over an equatorial basin, and Δ the time lag. Coefficient k varies with the annual cycle state of the zonal wind and is *positive* for one-half of the year and *negative* the other. In a simplified mathematics notation, that would be

$$k(t) = \begin{cases} -|k| & \text{during summer, and} \\ +|k| & \text{during winter.} \end{cases} \tag{1.2}$$

In a similar way, one may model the M87 local negative feedback mechanism quantitatively with Eq. (1.1), by letting the coefficient k be zero for the whole year, except during the annual maximum convection:

$$k(t) = \begin{cases} -|k| & \text{during maximum convection, and} \\ 0 & \text{rest of the year.} \end{cases} \tag{1.3}$$

The common thread that runs through these models is that they are all local, that is, the dynamics for the biennial oscillation are all confined in a single basin/region, and there is only one first-order differential equation. Under this property, the *presence of the time delay,* Δ*, in the differential equation (1.1) is essential for obtaining an oscillation solution.* The annual cycle in coefficient k,

tions between *more than one region*, an idea initially explored by M87.

One important observational characteristic of atmospheric convection associated with the TBO over the Asian–Australian monsoon region is that it exhibits a distinctive spatial structure and seasonality (Meehl 1987, 1994). Anomalies in convection represented by outgoing longwave radiation start over the Indian monsoon region during the northern summer and propagate southeastward and reach to the Australian monsoon region in the subsequent northern winter. That is, the phase of TBO persists, and a strong Australian monsoon frequently follows a strong Indian monsoon. Such spatial and seasonal characteristics of TBO are not addressed by the local air–sea feedback mechanisms proposed by M87 and C98. It may require remote air–sea–land interaction processes, processes that involve the Asian–Australian monsoon, large-scale east–west circulation, and tropical Pacific and Indian Oceans. M87 also proposed a remote forcing mechanism. The key ingredient is that the SSTA in the eastern Pacific induces an anomalous east–west circulation that further changes the strength of the South Asian monsoon. From a different perspective, Chang and Li (2000, hereafter CL00) emphasized the role of the monsoon in changing the east–west circulation and eastern Pacific SST, not the other way around. They argued that a small cold SSTA (order of -1 K; Ropelewski et al. 1992) in the eastern Pacific cold tongue is much less likely to play a role in pulling air mass out of the Asian monsoon region through the east–west circulation. To demonstrate the active role of the Asian–Australian monsoon on a TBO cycle, they developed a 5-box coupled ocean–atmosphere model that allows interactions among the South Asian and Australian monsoon regions and the equatorial Indian, western and eastern Pacific Oceans. The essential physical processes in the CL00 model include the monsoon-induced large-scale east–west circulation, SST–monsoon feedback, Walker cells over the equatorial Indian and Pacific Oceans, wind–evaporation–SST feedback, and ocean thermocline variation in the Pacific. The model is capable, *without a priori specification of time delays*, of simulating not only a biennial oscillation but also the phase relation between South Asian and Australian monsoons.

The objective of this study is twofold. First we pursue the analytical solution of the CL00 model by simplifying the model into a pair of homogeneous first-order differential equations, which are piecewise in time. The simplified model is then analyzed using linear differential calculus to explain the fundamental cause of TBO, from both mathematical and physical points of view. Second, we examine the sensitivity of the model solution to both internal coupling coefficients and external basic-state parameters in an attempt to understand the possible mechanisms that cause the irregularity of TBO.

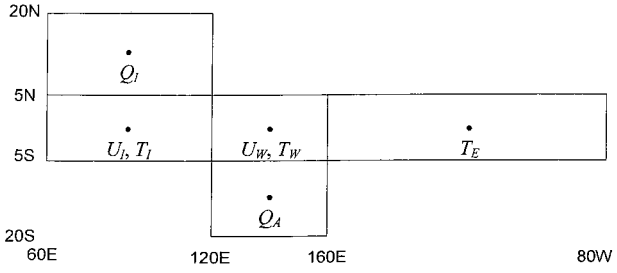

FIG. 2. Schematic diagram of the 5-box model of CL00.

2. Analysis of the 5-box model

The dynamic framework of the current model is intended to be similar to the CL00 model. Along the equator the ocean is divided into three regions (see Fig. 2), representing the equatorial Indian Ocean, western Pacific, and eastern Pacific, respectively. The rates of time change of the Indian Ocean and western Pacific SST anomalies are given by

$$\frac{dT_I}{dt} = \left[-\lambda\Delta\overline{q}_I\frac{\overline{U}_I}{V_0} - \overline{T}_I^{(x)}\frac{\alpha}{\rho hr} + \overline{T}_I^{(z)}\frac{(H-h)\beta\alpha}{\rho hr^2}\right]U_I - \left(\lambda V_0\kappa + \frac{\overline{w}_I}{h}\right)T_I, \tag{2.1a}$$

$$\frac{dT_W}{dt} = \left[-\overline{T}_C^{(x)}\frac{\alpha}{\rho hr} - \overline{T}_W^{(z)}\frac{2h(H-h)}{L_{\mathrm{EW}}} - \frac{\overline{w}_W\gamma\alpha L_{\mathrm{EW}}}{2\rho g' Hh}\right]U_C + \left[-\lambda\Delta\overline{q}_W\frac{\overline{U}_W}{V_0} + \overline{T}_W^{(z)}\frac{(H-h)\beta\alpha}{\rho Hr^2}\right]U_W - \left(\lambda V_0\kappa + \frac{\overline{w}_W}{h}\right)T_W, \tag{2.1b}$$

where U and w denote the surface zonal wind and ocean vertical velocity at the base of the mixed layer, respectively; Δq denotes air–sea specific humidity difference; $T^{(x)}$ and $T^{(z)}$ represent zonal and vertical ocean temperature gradients; and subscripts I, W, and C stand for the equatorial Indian Ocean, western, and central Pacific, respectively. An overbar denotes the annual-mean basic-state variable. In this simple dynamic system, the time tendency of SSTA in the equatorial Indian Ocean and western Pacific depends on various dynamic and thermodynamic processes including horizontal and vertical temperature advection and surface wind–evaporation feedback. Table 1 lists the meaning and value of the model key parameters.

Following CL00, the surface zonal winds over the equatorial Indian and Pacific oceans are determined by convective heating anomalies over the Indian and Australian monsoon regions (which in turn depends on anomalous low-level moisture convergence) and SST-dependent eastern and western Walker cells. Thus the surface zonal winds, U, are given by

TABLE 1. The list of key parameters of the coupled model.

Parameters		Value
Ocean thermocline mean depth	H	150 m
Ocean mixed layer mean depth	h	50 m
Reduced gravity	g'	0.015 m s^{-2}
SST–thermocline feedback coefficient	γ	0.18 K m^{-1}
SST–specific humidity constant	κ	7×10^{-4} K^{-1}
Rayleigh atmospheric friction coefficient	ε	1×10^{-5} s^{-1}
Oceanic Ekman layer friction coefficient	r	1×10^{-5} s^{-1}
Air–sea humidity difference	$\Delta\overline{q}$	5.6×10^{-3}
Half-length of Pacific basin	L_{EW}	8×10^{6} m
Indian Ocean annual mean zonal wind speed	$\overline{U}_I$	3 m s^{-1}
Western Pacific annual mean zonal wind speed	$\overline{U}_W$	0 m s^{-1}
Mean constant surface wind speed	V_0	4 m s^{-1}
Indian Ocean mean upwelling speed	$\overline{W}_I$	2×10^{-6} m s^{-1}
Western Pacific Ocean mean upwelling speed	$\overline{W}_W$	2×10^{-6} m s^{-1}
Indian Ocean mean zonal temperature gradient	$\overline{T}_I^{(x)}$	2×10^{-7} K m^{-1}
Central Pacific mean zonal temperature gradient	$\overline{T}_C^{(x)}$	-5×10^{-7} K m^{-1}
Indian Ocean mean vertical temperature gradient	$\overline{T}_I^{(z)}$	1×10^{-2} K m^{-1}
West Pacific mean vertical temperature gradient	$\overline{T}_W^{(z)}$	$1 \times 10^{-}$

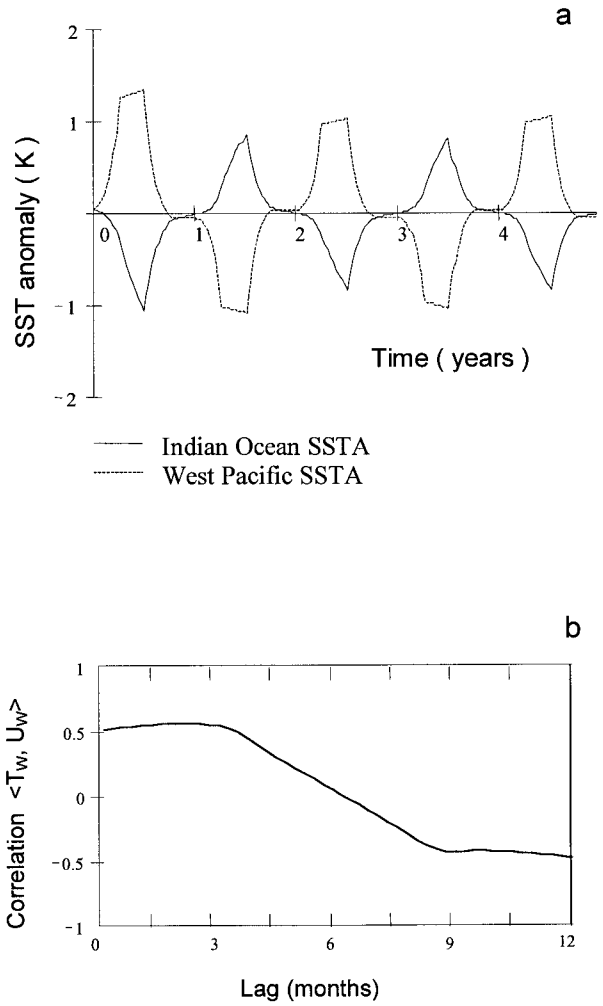

FIG. 3. (a) The simulated TBO in the simplified dynamic model [Eq. (2.5)]; (b) the lagged correlation between the western Pacific SST and zonal wind anomalies.

(because spring and autumn have the same coefficients), in the following form:

$$\frac{\partial}{\partial t}\begin{bmatrix} T_I \\ T_W \end{bmatrix} = \begin{bmatrix} a & b \\ c & d \end{bmatrix}\begin{bmatrix} T_I \\ T_W \end{bmatrix}. \tag{2.6}$$

The solution of (2.5) can be obtained from the solutions of (2.6) for each season, joined in time, where the initial values of each seasonal equations are equal to the final values of the previous season solutions. A complete analytical treatment of linear system of first-order differential equation (2.6) can be found in mathematical texts (e.g., see Grossman and Derrick 1988), and a summary, relevant to this work, is given in the appendix. In this section, we will make use of the results in the appendix. [where T_I corresponds to $x(t)$ and T_W to $y(t)$] to analyze the simple dynamic system (2.5), whose seasonal coefficients are given in Table 2.

The seasonal values of the coefficients of the simplified coupled model are plotted on the regime diagram in Fig. 4. (A complete description of the regimes of the linear system can be found in the appendix.) The model is in the *saddle point regime* (the middle graph of Fig. A1) during spring, autumn, and winter, and in the stable focus regime (the left graph of Fig. A2) during summer. To explain the biennial oscillation observed in the numerical evolution of the simple dynamic system (2.5), it is necessary to examine analytically the behavior of the model in each season, particularly in the winter and summer periods.

TABLE 2. The coefficients for the simplified TBO model for different seasons.

Seasons	a	b	c	d
Winter	−3.15	−4.06	0	12.87
Spring	−3.15	−4.06	0	0.27
Summer	−13.04	−4.06	13.34	0.27
Autumn	−3.15	−4.06	0	0.27

During winter, we observe a few relationships among the coefficients in Table 2: coefficient b is negative, coefficient c is zero, and coefficient d is greater than coefficient a. The reason that coefficient c is null is that in this simplified coupled model, the Indian Ocean SST does not affect that of the western Pacific during spring, autumn, and in particular winter. From Eqs. (A.7a) and (A.9a), the asymptote G_+ and G_- must take on the values of the second pair in Eq. (A.10) because $\lambda_+ = d$ and $\lambda_- = a$. Hence, asymptote G_- has a zero gradient while asymptote G_+ has a negative gradient. The implication of this result is that when T_W is negative (positive), it will continue to be more negative (positive) while T_I will either be flipped over from negative (positive) to positive (negative)

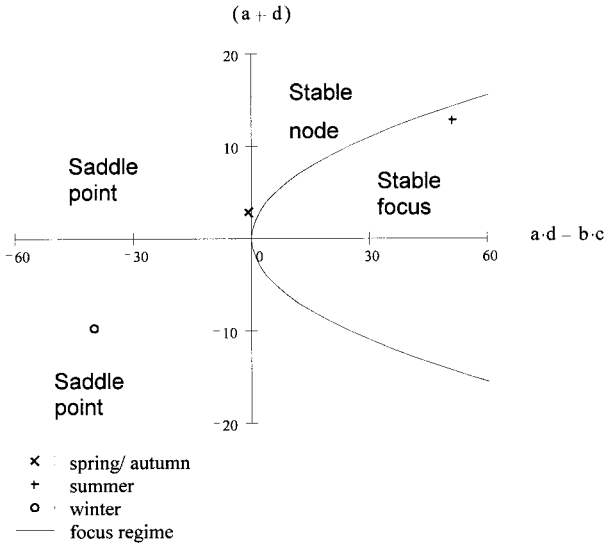

FIG. 4. The regime diagram for the simple coupled model and the standard parameter regime for the northern spring, summer, autumn, and winter.

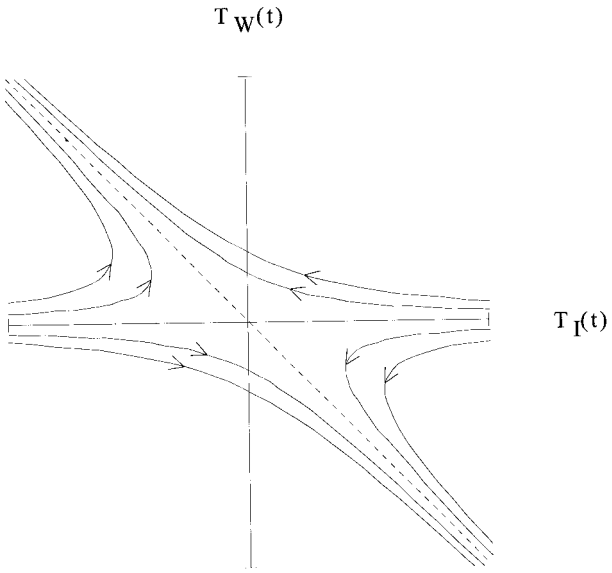
$T_W(t)$
$T_I(t)$

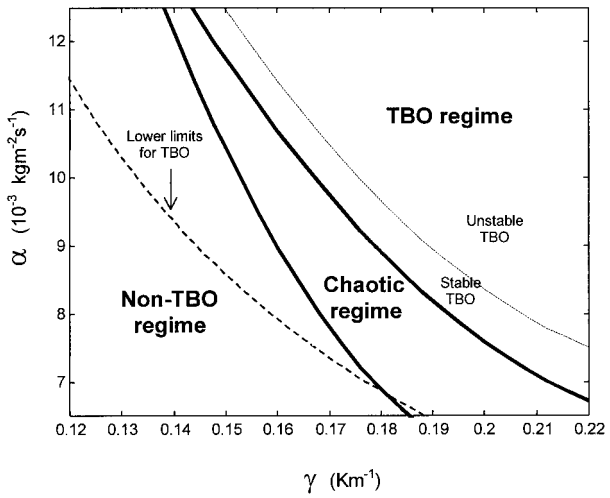

FIG. 7. Dependence of the model oscillation regime on the air–sea coupling coefficient, α, and the SST–thermocline feedback coefficient, γ.

coupling coefficient, α, and the SST–thermocline feedback coefficient, γ. The former links the surface wind stress with the oceanic current, while the latter connects the thermocline displacement with the change of subsurface ocean temperature (which may further feed back to SSTA through anomalous vertical temperature advection).

The model (2.5) is rewritten to explicitly include the air–sea coupling coefficient, α, and the SST–thermocline coefficient, γ, as parameters. An ensemble of solutions is obtained by varying, in steps, α from 6×10^{-3} to 13×10^{-3} kg m^{-2} s^{-1} and γ from 0.12 to 0.22 K m^{-1}. The frequency and growth rate of each time series solution are then calculated based on a least squares method, with the specification of the following mathematical formula: $Y(t) = Y_0 \cos(\omega t - \delta_0) \exp(-\sigma t)$, where ω denotes the frequency, σ the growth rate, Y_0 the amplitude, and δ_0 the initial phase.

Figure 7 clearly demonstrates that with the changes of internal coupling coefficients, the simple dynamic system undertakes different regimes, for instance, from an unstable to a stable TBO regime or from a TBO regime to a chaotic regime or a non-TBO (annual oscillation) regime. Thus this sensitivity experiment demonstrates that both processes are critical for obtaining the TBO. In the lower left-hand corner, where air–sea coupling is relatively weak, the model exhibits a nonbiennial oscillatory behavior, with a period of 1 yr (Fig. 8a). In the middle, solutions are much more irregular, exhibiting a chaotic oscillation regime (Fig. 8b). The stable and growing biennial oscillatory behavior is in the upper right-hand corner where both the air–sea coupling and the SST–thermocline feedback coefficients are sufficiently high (Fig. 8c).

A lower bound (i.e., a necessary condition) for the biennial oscillatory behavior can be derived analytically by considering the model's summer regime in Fig. 4.

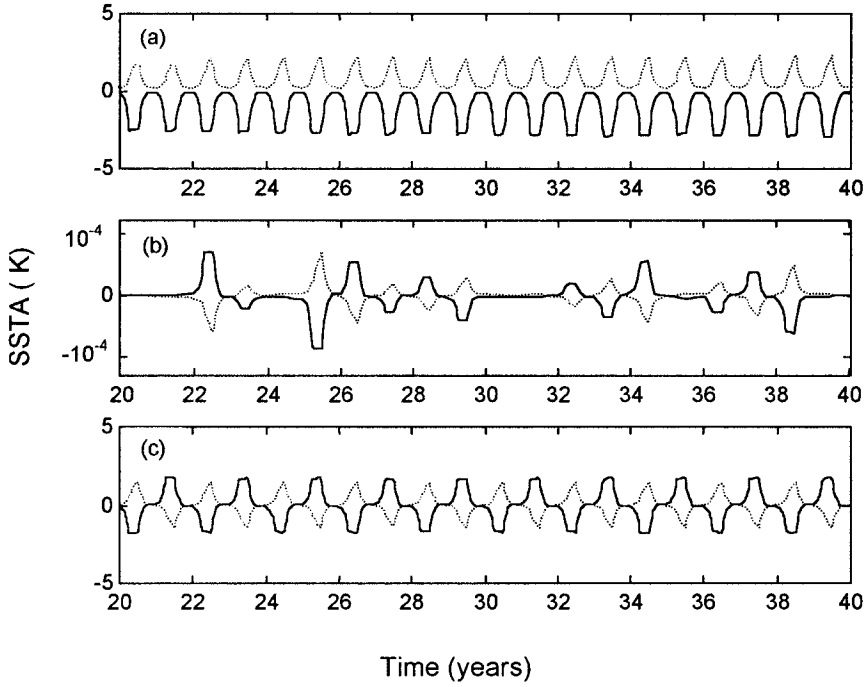

FIG. 8. Time series of the model SSTA (solid line: western Pacific, dashed line: Indian Ocean) in (a) a non-TBO (annual oscillation) regime ($\alpha = 13.4 \times 10^{-3}$ kg m^{-2} s^{-1} and $\gamma = 0.12$ K m^{-1}), (b) a chaotic regime ($\alpha = 9.1 \times 10^{-3}$ kg m^{-2} s^{-1} and $\gamma = 0.1785$ K m^{-1}), and (c) a TBO regime ($\alpha = 8 \times 10^{-3}$ kg m^{-2} s^{-1} and $\gamma = 0.2075$ K m^{-1}).

As stated previously, one of the criteria for oscillation is that during summer, the model must be in the stable focus regime. This means that the summer parameter point must be beneath the focus regime boundary curve (see Fig. 4). Therefore characteristic equation (A.7) in the appendix must have imaginary roots:

$$(a + d)^2 - 4(ad - bc) < 0. \tag{3.1}$$

Substituting (3.1) with the standard parameters in summer, we have a quadratic equation for γ as the left-hand side of the condition:

$$443 \times 10^4\,\alpha^2\gamma^2 + (-127 \times 10^3\,\alpha + 149 \times 10^4\,\alpha^2)\gamma + 127 + 206 \times 10^2\,\alpha - 450 \times 10^2\,\alpha^2 < 0. \tag{3.2}$$

Since α is of the order of 10^{-3} kg m^{-2} s^{-1}, we can expand α into a power series and retain the first two terms without any loss of significant digits:

$$\left(\gamma - \frac{0.00103}{\alpha} + 0.0304\right)\left(\gamma - \frac{0.0277}{\alpha} + 0.367\right) < 0. \tag{3.3}$$

Thus the necessary condition for the biennial oscillation would be

$$\gamma > \frac{0.00103}{\alpha} + 0.030 \quad \text{and}$$

$$\gamma < \frac{0.0277}{\alpha} + 0.367. \tag{3.4}$$

Since the second condition in (3.4) is always satisfied in the real world, the first condition represents a lower limit for the biennial oscillation. In other words, it is a necessary (but not sufficient) condition for the TBO to occur. This condition is demarcated by a thick dashed line in Fig. 7. It implies that the TBO regime must appear above the line.

In addition to α and γ, the model is also sensitive to other internal parameters such as the atmospheric Rayleigh friction coefficient, ε, and the depth of the ocean mixed layer, h, as shown in Fig. 9. With the slight change of these parameters, the model solution can shift from a TBO to a non-TBO regime or from an oscillation to a chaotic regime, leading to the irregularity of the TBO. It is also noted that a common feature from those sensitivity experiments is that the model always undergoes a rapid decay during the chaotic transition from a regular TBO mode to a non-TBO mode or vice versa.

b. Sensitivity to basic-state changes

In the above section, we have shown that the model may switch from an oscillatory to a nonoscillatory mode or from a TBO mode to annual oscillation mode with the change of internal parameters. Specifically, when the summer parameter point in Fig. 4 shifts from a stable

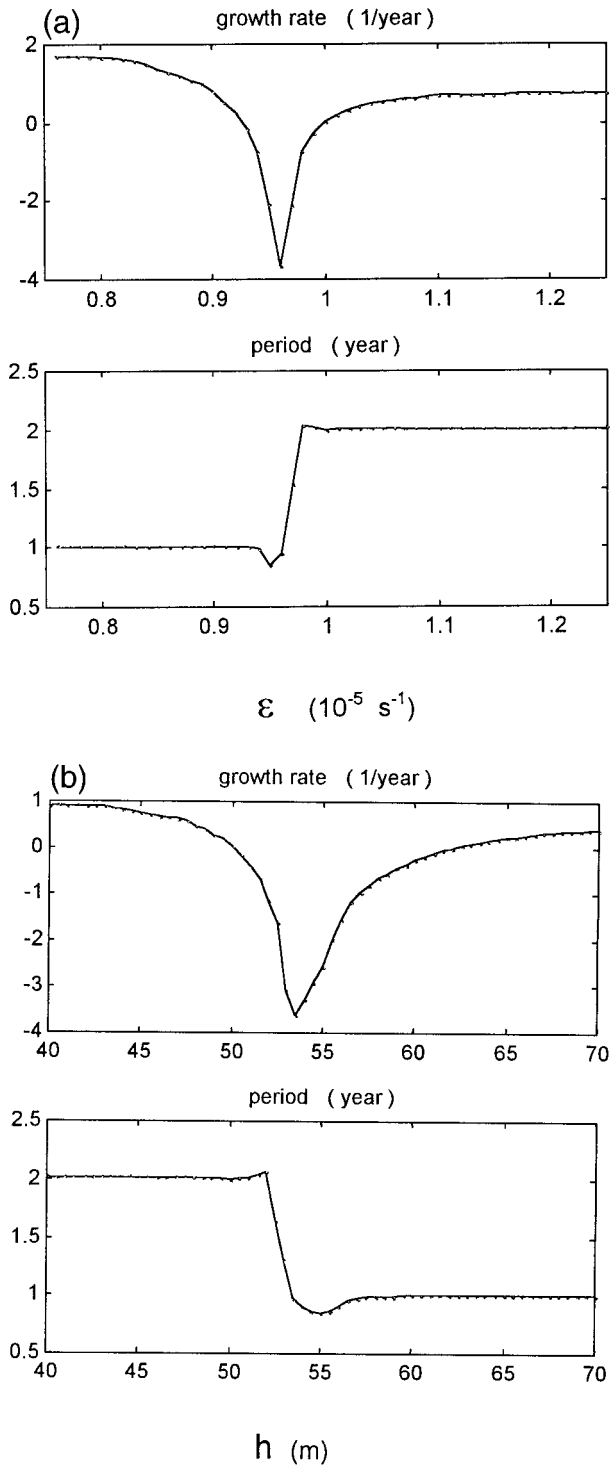

FIG. 9. Dependence of the growth rate and oscillation period on (a) atmospheric Rayleigh friction coefficient and (b) the ocean mixed layer depth.

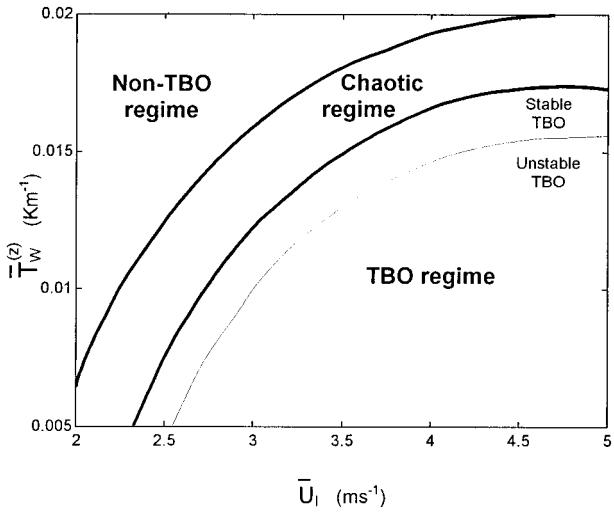

FIG. 10. Dependence of the model oscillation regime on the western Pacific mean vertical temperature gradient, $\overline{T}_W^{(z)}$, and Indian Ocean mean surface wind speed, $\overline{U}_I$.

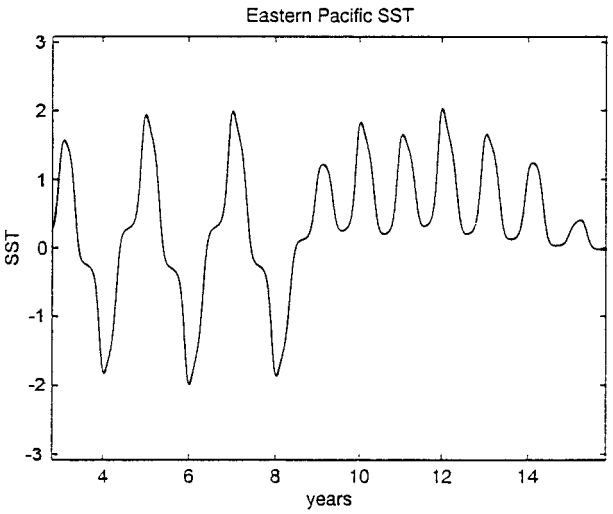

FIG. 11. Temporal evolution of the eastern equatorial Pacific SSTA undergoing a bifurcation from a regular TBO mode to an abnormal mode resembling the prolonged warming episode during the early 1900s. A slowly evolving interdecadal (with a 15-yr period) basic-state wind is specified.

focus regime into a stable node regime, biennial oscillation is not possible. In this section we further examine the sensitivity of model solution to external parameters such as the basic state of the coupled ocean–atmosphere system.

Figure 10 illustrates the model oscillation regimes under different basic-state parameter values for the zonal wind over the Indian Ocean and the upper-ocean vertical temperature gradient in the western Pacific. Note that the model solution is very sensitive to the external parameters. With a small change of these basic-state parameters, the model may undertake a bifurcation from a TBO mode to a chaotic regime or to a non-TBO (annual oscillation) regime.

The sensitivity of the model oscillatory behavior to both the basic state and internal parameters poses an interesting question: are they the causes of irregularity of TBO? As these parameters represent the measure of dynamical processes of the complex physical world, they may change from time to time. For instance, the interactions with other tropical systems such as the Madden–Julian oscillation (MJO) and ENSO may interrupt or break the regular cycle of a TBO by changing the sign of SSTA either in the Indian Ocean or the western Pacific from a positive (negative) to a negative (positive)

magnitude and change in sign in the northern summer. Under such a scenario, the model TBO exhibits a characteristic spatial pattern and seasonal progression, with a strong Australian monsoon following a strong South Asian monsoon.

Analogous to the El Niño delayed action oscillator that depends on equatorial oceanic wave propagation, the current TBO monsoon oscillator depends on remote and local ocean–atmosphere interactions in the Asian–Australian monsoon region and the equatorial Indian Ocean and western Pacific. On one hand, the annual cycle of the Asian–Australian monsoon, as a pacemaker, strongly regulates the TBO mode, so that the biennial oscillation locks its phase into the seasonal cycle. On the other hand, the feedbacks between the Indian Ocean SSTA and the monsoon, between the surface wind and evaporation, and between the wind stress and ocean thermocline contribute to the year-to-year variation of the coupled air–sea modes. Among various air–sea interaction processes, the impact of the Asian monsoon on the Pacific SSTA through large-scale east–west circulation and the influence of the western Pacific/maritime continent SSTA on the strength of the western branch of the Walker cell over the Indian Ocean are most critical. It is suggested that the origin of the TBO may arise from ocean–atmosphere interactions within the monsoon sector in the Tropics.

The possible influence of midlatitude circulation on the tropical biennial oscillation has been proposed by Meehl (1997) based on the diagnosis of output of a coupled ocean–atmosphere model. The key element of this proposed mechanism is the linkage between anomalous tropical heating and midlatitude circulation patterns. However, such a linkage is beyond the scope of the current study. It deserves further observational analyses.

An essential difference between the current 5-box model and previous conceptual TBO models such as those discussed in the first section is that the current model considers the interactions among multiple regions whereas the previous models considered only local air–sea interaction processes. Because of locality, some forms of time delay between atmosphere (such as surface wind) and ocean (SST) are required (see discussions in section 1), in order to obtain an oscillatory solution. As shown by this study, such a constraint is neither dynamically consistent nor necessary. The time delay between the surface wind and SST in the western Pacific as observed by C98 is a result rather than a cause of TBO. It results from both remote and local ocean–atmosphere interactions, interactions that involve the Asian–Australian monsoon and associated large-scale east–west circulation, evaporation–wind–SST feedback, and subsurface ocean temperature changes.

The sensitivity analysis of the current model reveals that the model solution is sensitive to changes in both internal parameters such as air–sea coupling and atmospheric friction coefficients and external parameters such as the basic-state zonal wind and upper-ocean vertical temperature gradient. It is found that a necessary condition for the model to be in the TBO regime is that two crucial air–sea coupling coefficients, reflecting the surface wind–ocean current and the subsurface temperature–ocean thermocline relations, must be sufficiently large and within reasonable ranges. With the small change of both the internal and external parameters, the model may undergo a bifurcation from a regular TBO regime to a non-TBO (either chaotic or annual oscillation) regime. When the basic state varies slowly on the interdecadal timescale, the model SST experiences a continuous warming pattern, similar to the prolonged warm episode in the equatorial Pacific during the early 1990s. However, it is important to note that the observed behavior in the early 1990s is unique for the last century whereas the low-frequency fluctuation of the wind might be ubiquitous throughout the record. This implies that there are likely other factors that may contribute to this unique feature. It is anticipated that the complex behavior of the observed TBO may arise from its interactions with motions at other scales such as Madden–Julian oscillation, ENSO, or synoptic-scale disturbances. These interactions may alter the model oscillation regimes and give rise to the irregular oscillation behavior of the TBO.

Acknowledgments. We wish to thank Dr. N. Nicholls and an anonymous reviewer for their constructive comments. The work was supported by the National Science Foundation under Grant ATM 9613746, and by the International Pacific Research Center that is sponsored in part by the Frontier Research System for Global Change. This is School of Ocean and Earth Sciences and Technology Contribution Number 5297 and International Pacific Research Center Contribution Number 65.

APPENDIX

Analytical Solution for Linear Homogeneous First-Order Differential Equations

In its most general form, a linear system of homogeneous first-order differential equations represented by

$$\frac{\partial}{\partial t}\mathbf{T}(t) = \mathbf{M}\mathbf{T}(t), \tag{A.1}$$

where $\mathbf{T}(t)$ is the vector of variables of concern and $\mathbf{M}$ is the matrix of constant coefficients, has a solution

$$\mathbf{T}(t) = \exp(t\mathbf{M})\mathbf{T}(t_0), \tag{A.2}$$

where t_0 is the time of the initial conditions and exp( ) is the matrix exponential function

$$\exp(t\mathbf{M}) = \mathbf{I} + t\mathbf{M} + \frac{t^2}{2!}\mathbf{M}^2 + \frac{t^3}{3!}\mathbf{M}^3 + \cdots. \tag{A.3}$$

It is a general property that for real t and n-by-n square matrix $\mathbf{M}$, the series (A.3) is convergent.

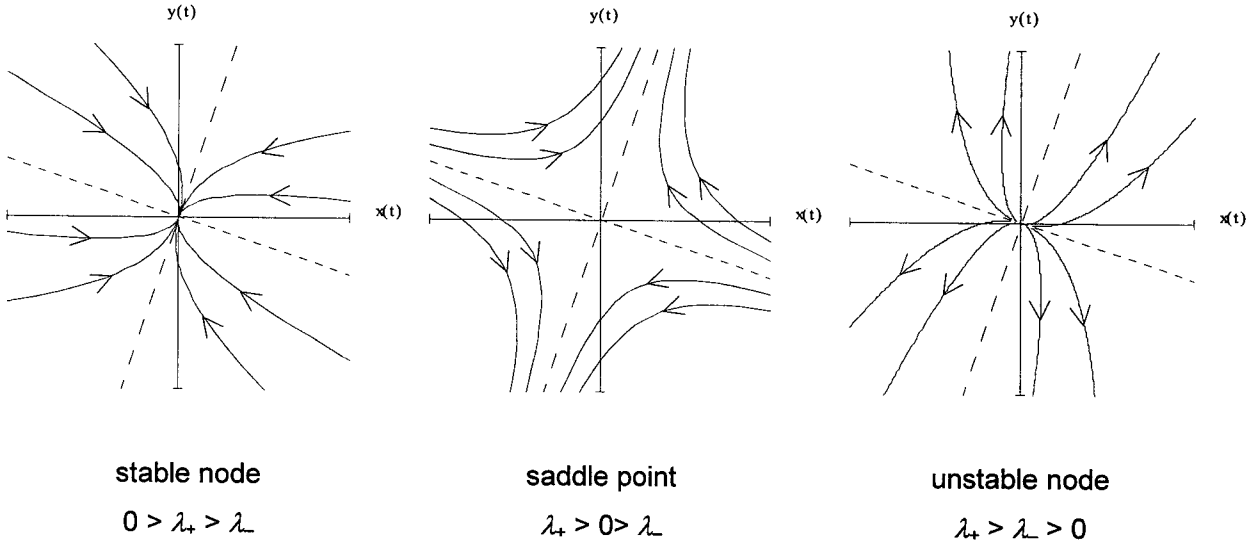

FIG. A1. The phase diagrams for real eigenvalue cases (long dashed line: asymptote G_+; short dashed line: asymptote G_-).

In the following discussion, we consider the solution of two *independent variables initial value problems* and its orbits in phase space. Equation (A.1) is then

$$\frac{\partial x}{\partial t} = ax + by \qquad \frac{\partial y}{\partial t} = cx + dy. \tag{A.4}$$

The linear systems of differential equations with initial values lend themselves particularly well to *Laplace transform* techniques. The Laplace transformation of (A.4) is

$$sX - x_0 = aX + by \qquad sY - y_0 = cX + dy, \tag{A.5}$$

where s, X, and Y are the Laplace transform of t, x, and y; x_0 and y_0 are the initial values of x and y at time t_0. The solution of (A.5) is

$$X = \frac{(s - d)x_0 + by_0}{s^2 - (a + d)s + (ad - bc)}$$

$$Y = \frac{cx_0 + (s - a)y_0}{s^2 - (a + d)s + (ad - bc)}. \tag{A.6}$$

If we define λ_+, λ_- [incidentally, they are also the eigenvalues of $\mathbf{M}$ in (A.1)] to be the roots of the characteristic equations

$$\lambda^2 - (a + d)\lambda + (ad - bc) = 0, \tag{A.7}$$

or equivalently,

$$(\lambda - a)(\lambda - d) = bc, \tag{A.7a}$$

then it plainly appears that (A.6) can be written as

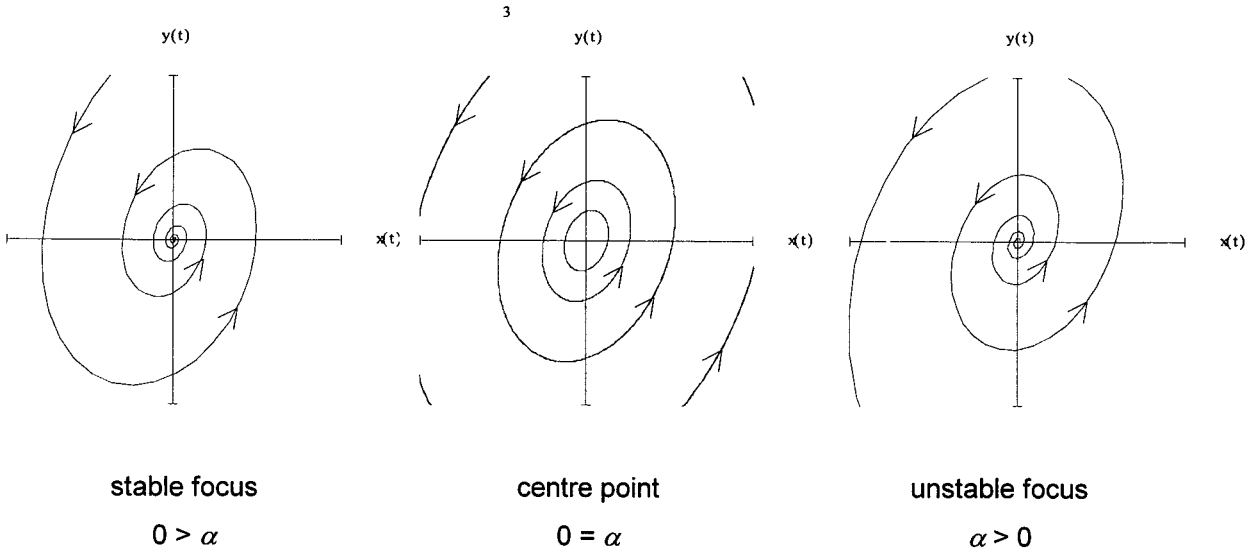

FIG. A2. The phase diagrams for complex eigenvalue cases.

$$X = \frac{(s-d)x_0 + by_0}{(s-\lambda_+)(s-\lambda_-)}$$

$$Y = \frac{cx_0 + (s-a)y_0}{(s-\lambda_+)(s-\lambda_-)}. \tag{A.8}$$

Considering only the solution of the general *nondegenerate* linear system (i.e., $\lambda_+ \neq \lambda_-$), the inverse Laplace transform of (A.8) is

$$x(t) = \frac{(\lambda_+ - d)x_0 + by_0}{(\lambda_+ - \lambda_-)}e^{\lambda_+ t} - \frac{(\lambda_- - d)x_0 + by_0}{(\lambda_+ - \lambda_-)}e^{\lambda_- t}$$

$$y(t) = \frac{cx_0 + (\lambda_+ - a)y_0}{(\lambda_+ - \lambda_-)}e^{\lambda_+ t} - \frac{cx_0 + (\lambda_- - a)y_0}{(\lambda_+ - \lambda_-)}e^{\lambda_- t}. \tag{A.9}$$

This is the general nondegenerate solution for (A.4). It is illuminating to examine solutions (A.9) in the phase space and we shall consider separately the cases where the roots of (A.7) are real and complex.

a. Case of real roots, $(a+d)^2 \geq 4(ad-bc)$

The phase space diagram of (A.9) can be obtained by first looking at the asymptotes as time tends to infinity and as time originates from minus infinity. Assume, without a loss of generality,

$$\lambda_+ > \lambda_-. \tag{A.9a}$$

From (A.9), we see that the asymptote gradients, G_+ and G_-,

$$G_+ \equiv \lim_{t\to\infty}\frac{y(t)}{x(t)} = \frac{cx_0 + (\lambda_+ - a)y_0}{(\lambda_+ - d)x_0 + by_0}$$

$$G_- \equiv \lim_{t\to-\infty}\frac{y(t)}{x(t)} = \frac{cx_0 + (\lambda_- - a)y_0}{(\lambda_- - d)x_0 + by_0}. \tag{A.10}$$

Using (A.7a), (A.10) can be reduced, respectively, to

$$G_+, G_- = \begin{cases} \dfrac{c}{\lambda_+ - d}, & \dfrac{\lambda_- - a}{b} \quad \text{if } (\lambda_+ \neq d) \text{ and } (\lambda_- \neq a), \text{ or} \\ \dfrac{\lambda_+ - a}{b}, & \dfrac{c}{\lambda_- - d} \quad \text{if } (\lambda_+ \neq a) \text{ and } (\lambda_- \neq d). \end{cases} \tag{A.11}$$

If both λ_+, λ_- are negative, then from (A.9), it is plain that both $y(t)$ and $x(t)$ will tend to infinity with time and to zero with reverse time (i.e., $t \to -\infty$), resulting in a *stable node* (Fig. A1). On the other hand, if both λ_+, λ_- are positive, then the solutions tend to zero with time and to infinity with reverse time, forming an *unstable node.* If the eigenvalues are of opposite signs, then the solutions tend to infinity with both time and its reversal, having a *saddle point* for the origin.

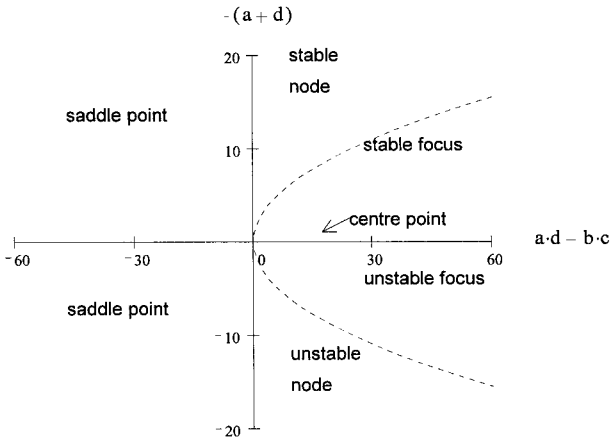

FIG. A3. The regime diagram for the linear differential equation system.

b. Case of complex roots, $(a+d)^2 < 4(ad-bc)$

If the eigenvalues are complex, then we can substitute $\lambda_{+,-} = \alpha \pm i\beta$ into (A.9) giving

$$x(t) = e^{\alpha t}\left[x_0\cos(\beta t) + \frac{(\alpha - d)x_0 + by_0}{\beta}\sin(\beta t)\right]$$

$$y(t) = e^{\alpha t}\left[y_0\cos(\beta t) + \frac{cx_0 + (\alpha - a)y_0}{\beta}\sin(\beta t)\right]. \tag{A.12}$$

If α is negative, then from (A.11) the solution tends to zero, and its origin is a *stable focus* (Fig. A2). If, however, α is greater than zero, the solutions tend to infinity, forming an *unstable focus.* For $\alpha = 0$, the solutions are periodic and the origin is a *center point.*

The dependence of the solution type on the roots of the characteristic equation (A.9), and hence on the coefficients a, b, c, and d, is given in Fig. A3. The dividing curve between the foci and the nodes are given by the equation $(a+d)^2 - 4(ad-bc) = 0$, while the regime for the center point solutions is the positive horizontal axis.

REFERENCES

Battisti, D. S., and A. C. Hirst, 1989: Interannual variability in a tropical atmosphere–ocean model: Influence of the basic state, ocean geometry and nonlinearity. *J. Atmos. Sci,* **46,** 1687–1712.

Brier, G. W., 1978: The quasi-biennial oscillation and feedback processes in the atmosphere-ocean-earth system. *Mon. Wea. Rev.*, **106,** 938–946.

Chang, C.-P., and T. Li, 2000: A theory for the tropospheric biennial oscillation. *J. Atmos. Sci.,* **57**, 2209–2224.

——, Y. Zhang, and T. Li, 2001: Interannual and interdecadal variations of the East Asian summer monsoon and tropical Pacific SSTs. Part I: Roles of the subtropical ridge. *J. Climate,* **13,** 4310–4325.

Clarke, A. J., X. Liu, and S. V. Gorder, 1998: Dynamics of the biennial oscillation in the equatorial Indian and far western Pacific Oceans. *J. Climate,* **11,** 987–1001.

Grossman, S. I., and W. R. Derrick, 1988: *Advanced Engineering Mathematics.* Harper & Row, 127–187.

Gu, D., and S. G. H. Philander, 1997: Interdecadal climate fluctuations that depend on exchanges between the Tropics and extratropics. *Science,* **275,** 805–807.

Lau, K.-H., and P. J. Shen, 1988: Annual cycle, quasi-biennial oscillation, and Southern Oscillation in global precipitation. *J. Geophys. Res.*, **93,** 10 945–10 988.

——, and S. Yang, 1996: The Asian monsoon and predictability of the tropical ocean–atmosphere system. *Quart. J. Roy. Meteor. Soc.*, **122,** 945–957.

Meehl, G. A., 1987: The annual cycle and interannual variability in the tropical Pacific and Indian Ocean region. *Mon. Wea. Rev.*, **115,** 27–50.

——, 1994: Coupled ocean-atmosphere-land processes and South Asian monsoon variability. *Science,* **265,** 263–267.

——, 1997: The south Asian monsoon and the tropospheric biennial oscillation (TBO). *J. Climate,* **10,** 1921–1943.

Mooley, D. A., and B. Parthasarathy, 1984: Fluctuations in all-India summer monsoon rainfall during 1871–1978. *Climatic Change,* **6,** 287–301.

Nicholls, N., 1978: Air–sea interaction and the quasi-biennial oscillation. *Mon. Wea. Rev.*, **106,** 1505–1508.

——, 1979: A simple air–sea interaction model. *Quart. J. Roy. Meteor. Soc.*, **105,** 93–105.

——, 1984: The Southern Oscillation and Indonesia sea surface temperature. *Mon. Wea. Rev.*, **112,** 424–432.

Rasmusson, E. M., and T. H. Carpenter, 1982: The relationship between the eastern Pacific sea surface temperature and rainfall over India and Sri Lanka. *Mon. Wea. Rev.*, **110,** 354–384.

Ropelewski, C. F., M. S. Halpert, and X. Wang, 1992: Observed tropospheric biennial variability and its relationship to the Southern Oscillation. *J. Climate,* **5,** 594–614.

Shen, S., and K.-M. Lau, 1995: Biennial oscillation associated with the east Asian monsoon and tropical sea surface temperatures. *J. Meteor. Soc. Japan,* **73,** 105–124.

Suarez, M. J., and P. S. Schopf, 1988: A delayed action oscillator for ENSO. *J. Atmos. Sci.,* **45,** 3283–3287.

Tian, S. F., and T. Yasunari, 1992: Time and space structure of interannual variations in summer rainfall over China. *J. Meteor. Soc. Japan*, **70,** 585–596.

Trenbenth, K. E., 1990: Recent observed interdecadal climate changes in the Northern Hemisphere. *Bull. Amer. Meteor. Soc.*, **71,** 988–993.

Wang, B., 1995: Interdecadal changes in El Niño onset in the last four decades. *J. Climate,* **8,** 267–285.

Webster, P. J., V. O. Magana, T. N. Palmer, J. Shukla, R. A. Tomas, M. Yanai, and T. Yasunari, 1998: Monsoons: Processes, predictability, and the prospects for prediction. *J. Geophys. Res.*, **103** (C7), 14 451–14 510.

Yasunari, T., 1990: Impact of the Indian monsoon on the coupled atmosphere/ocean system in the tropical Pacific. *Meteor. Atmos. Phys.,* **44,** 29–41.

——, and R. Suppiah, 1988: Some problems on the interannual variability of Indonesia monsoon rainfall. *Tropical Rainfall Measurements*, J. S. Theon and N. Fugono, Eds., Deepak, 113–122.

Zhang, Y., J. M. Wallace, and D. S. Battisti, 1997: ENSO-like interdecadal variability: 1900–93. *J. Climate,* **10,** 1004–1020.